



## OPEN Differences in different reconstruction algorithms for coronary CTA demonstrating pericoronary adipose tissue attenuation

Yuxuan Zhu, Jiajie Zhu, Xin Ding, Yingying Ge, Dejong Liu & Hongbing Ma✉

The Fat Attenuation Index (FAI) surrounding the coronary arteries, a sensitive biomarker for coronary inflammation, can be measured through standard Coronary Computed Tomography Angiography (CCTA). The aim of this study is to evaluate the differences in FAI as displayed on CCTA using three different reconstruction algorithms: high-level Deep Learning Image Reconstruction (DLIR-H), adaptive statistical iterative reconstruction-Veo at a level of 50% (ASiR-V50%), and Filtered Back Projection (FBP). Based on the presence or absence of plaque, the population was divided into the following groups: normal, no plaque, non-calcified plaque, mixed plaque, and calcified plaque. Each group was then further analysed according to the reconstruction algorithm, with three subgroups for each: DLIR-H, ASiR-V50%, and FBP. Attenuation values for pericardial adipose tissue, image noise, and the Fat Attenuation Index (FAI) of the three proximal coronary arteries were measured and evaluated for each of the three reconstruction algorithms. The attenuation values of pericardial adipose tissue measured by the three algorithms were not statistically different. However, the FAI measured by DLIR-H was the highest, followed by ASiR-V50%, with FBP yielding the lowest value; all differences were statistically significant. Meanwhile, DLIR-H demonstrated the strongest ability to reduce image noise, whereas FBP showed the weakest ability to do so. FAI varies significantly depending on the algorithm used. Therefore, standardised reconstruction protocols are essential in multicentre and longitudinal studies to ensure accurate, reproducible, and comparable FAI results.

**Keywords** Heart, Coronary CTA, Algorithm, Fat attenuation index

### Abbreviations

ASiR-V50%	Adaptive statistical iterative reconstruction-Veo at a level of 50%
CAD	Coronary artery disease
CCTA	Coronary CTA
DLIR-H	High-level deep learning image reconstruction
FAI	Fat attenuation index
FBP	Filtered back projection
HU	Hounsfield units
LAD	Left anterior descending artery
LCX	Left circumflex artery
RCA	Right coronary artery

The onset and progression of coronary atherosclerosis are associated with inflammation of the coronary vasculature. In the CANTOS study, anti-inflammatory therapy reduced cardiovascular events and validated the hypothesis of stable coronary artery disease (CAD) and residual coronary inflammation<sup>1</sup>. Therefore, early recognition of vascular inflammation and assessment of its extent can prevent the development of coronary heart disease and improve the prognosis of patients with the condition<sup>2</sup>. In 2017, Antonopoulos et al.<sup>3</sup> developed the Fat Attenuation Index (FAI) to quantify coronary inflammation, demonstrating its excellent sensitivity

Department of Radiology, Nanjing BenQ Medical Center, The Affiliated BenQ Hospital of Nanjing Medical University, Nanjing, Jiangsu Province, China. ✉email: mhb\_mj@126.com

and specificity in detecting tissue inflammation via positron emission tomography (PET) of tissue uptake of  $^{18}\text{F}$ -fluorodeoxyglucose.

The CRISP CT study<sup>4</sup> showed that the proximal right coronary artery can predict both all-cause and cardiac mortality. It identified an optimal cut-off value of  $-70.1$  HU per coronary FAI, determined using the receiver operating characteristic (ROC) curve for cardiac mortality over time, and found that  $\text{FAI} \geq -70.1$  HU indicates an increased risk of cardiac mortality. However, the generalisation of this threshold may be limited, as FAI is influenced by multiple factors, including: (1) technical factors (e.g., tube voltage<sup>5</sup>, CT scanner type<sup>6</sup>, contrast agent<sup>7</sup>), (2) biological factors (e.g., patient gender<sup>8</sup>, body mass index<sup>9</sup>), and (3) anatomical factors (e.g., coronary artery segmentation<sup>10</sup>). This led to the development of artificial intelligence-enhancing algorithms, such as the CaRi-HEART algorithm.

With advances in algorithms, deep learning image reconstruction (DLIR) is gradually replacing iterative reconstruction (IR) algorithms as the mainstay in coronary CTA (CCTA), as DLIR can improve image quality under low tube voltage conditions while simultaneously reducing radiation exposure and contrast dose<sup>11</sup>. Although Etter et al<sup>12</sup> demonstrated that IR algorithms lead to higher FAI values compared to traditional filtered back projection (FBP) algorithms, it remains unclear how deep learning reconstruction algorithms affect FAI values.

Therefore, the aim of this study was to evaluate the effects of three reconstruction algorithms—high-level DLIR (DLIR-H), adaptive statistical iterative reconstruction-Veo at a level of 50% (ASiR-V50%), and Filtered Back Projection (FBP)—on FAI in different patient populations, including the normal and coronary plaque populations.

## Materials and methods

This was a single-centre prospective study approved by the local hospital ethics committee.

### Study population

Between January 2024 and August 2024, 502 consecutive patients undergoing CCTA were included in the study. The following patients were excluded: (1) patients with allergy to iodinated contrast agents; (2) patients with clinical instability (e.g., acute myocardial infarction, decompensated heart failure, severe hypotension); (3) patients with severe hepatic or renal insufficiency; and (4) patients who had undergone stent implantation or coronary artery bypass grafting. Of these, 15 patients with stent implantation and 2 patients with bypass were excluded, leaving a total of 485 patients. Based on the presence or absence of plaques and the nature of the plaques, the patients were categorised into the following groups: normal, no plaque, non-calcified plaque, mixed plaque, and calcified plaque. Each group was further subdivided into DLIR-H, ASiR-V50%, and FBP subgroups.

### Coronary CTA scanning protocols and injection protocols

All patients were scanned using a 256-slice CT scanner (Revolution APEX CT, GE Healthcare, Waukesha, WI, USA) with a prospective electrocardiogram (ECG)-triggered axial scanning protocol. The standard tube voltage was set to 120 kV, with automatic tube current modulation (200–800 mA) and Smart Phase technology for automatic cardiac phase selection. The scanning range extended from the level of the tracheal bifurcation to the base of the heart, with the detector width adjusted to 12, 14, or 16 cm depending on the size of the patient's heart. The gantry rotation time was 0.28 s, with a slice thickness and reconstruction interval of 0.625 mm, and a  $512 \times 512$  reconstruction matrix. DLIR-H, ASiR-V50%, and FBP algorithms (GE Healthcare) were used to reconstruct the images, followed by the application of second-generation motion correction algorithms (SSF2, GE Healthcare) to minimise motion artefacts.

Fifty millilitres of preheated ( $37^\circ\text{C}$ ) Omnipaque contrast (350 mgI/ml, GE Healthcare) was injected at 5 ml/s into the antecubital vein using a dual-tip CT power injector (Stellant, Bayer), followed by a 40 ml saline flush at the same flow rate. A push-injection tracking technique was employed to ensure adequate contrast enhancement, with the region of interest (ROI) located in the descending aorta and a trigger threshold of 200 Hounsfield units (HU).

### Measurement of coronary artery attenuation values and image noise across different reconstruction algorithms

For images of the same patient reconstructed using different algorithms (DLIR-H, ASiR-V50%, and FBP), the attenuation value  $\pm$  standard deviation was measured at the level of the aortic root, aligned with the ostium of the left main coronary artery. The measured attenuation value was regarded as the mean coronary artery attenuation, while the standard deviation was used as an indicator of image noise in CCTA. The measurement procedure involved ensuring consistency in both the position and size of the ROI using the Clone function. The measurement area was set to  $2/3$  of the largest cross-sectional area of the vessel, avoiding the vessel wall, as well as calcified and non-calcified plaques. Each measurement was repeated three times, and the average value was taken, as shown in Fig. 1.

### Measurement of pericardial fat attenuation values for different reconstruction algorithms

For images of the same patient obtained using different reconstruction algorithms (DLIR-H, ASiR-V50%, and FBP), the attenuation value of the pericardial adipose tissue in front of the aortic root was measured at the level of the opening of the left main coronary artery. The measurement method involved ensuring consistency in both the position and size of the ROI using the Clone function. The measurement area was defined as the maximum fat area, with the measurement avoiding blood vessels and adjacent myocardial tissues. Each measurement was repeated three times, and the average value was taken, as shown in Fig. 1.

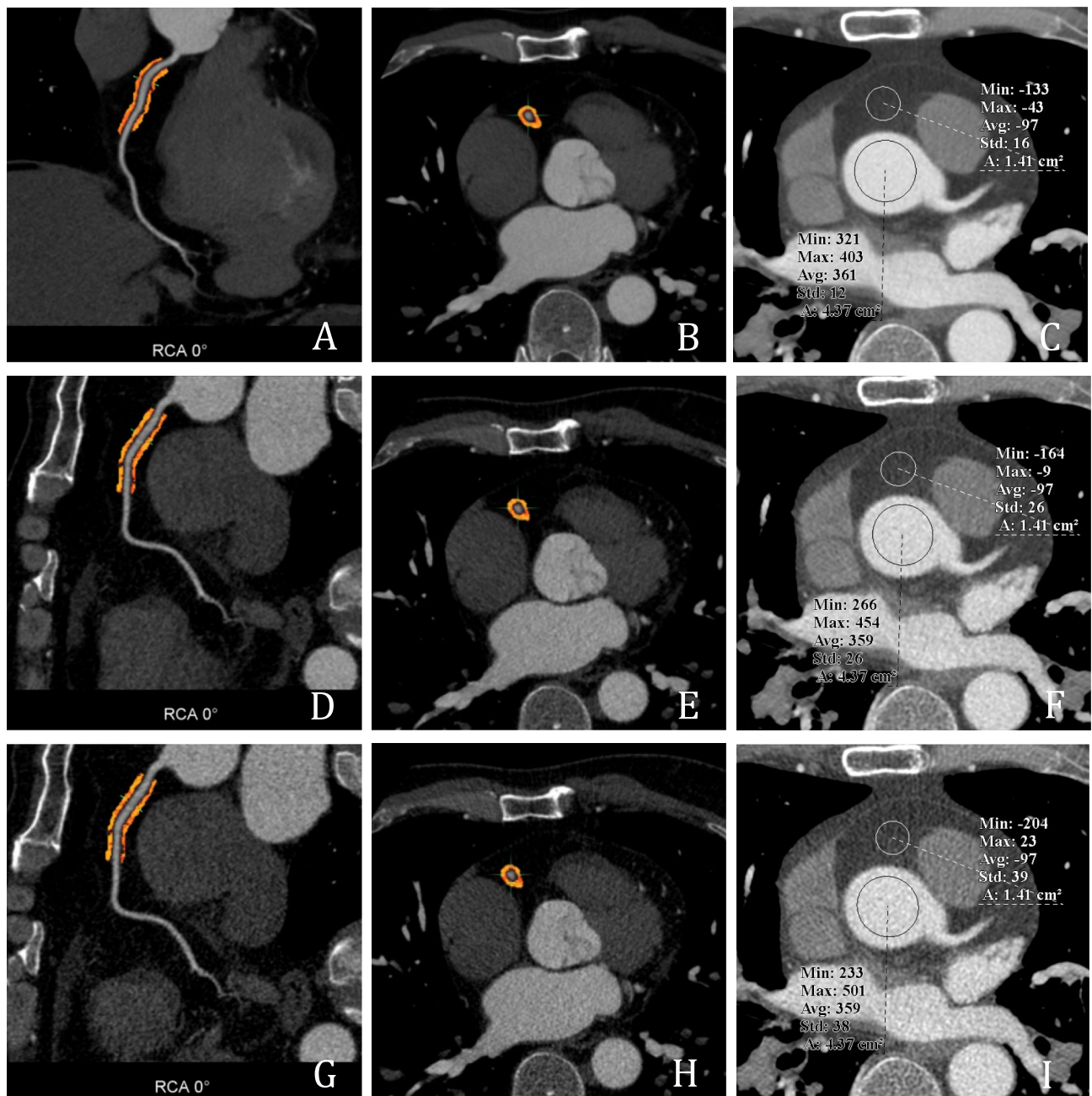


**Fig. 1.** Schematic of coronary FAI, image noise, and pericardial fat attenuation measurements. (a–c) show CCTA images reconstructed using the high-level deep learning image reconstruction (DLIR-H) algorithm. Figure displays the longitudinal diameter fat attenuation index (FAI) of the proximal right coronary artery (RCA) segment (10–50 mm), with an FAI value of  $-92$  HU. (b) shows the corresponding short-axis FAI. (c) demonstrates an image noise level of  $12$  HU and a pericardial fat attenuation value of  $-97$  HU at the level of the left main coronary artery. (d–f) present CCTA images reconstructed using the adaptive statistical iterative reconstruction-Veo at a level of  $50\%$  (ASiR-V50%) algorithm. (d) shows the longitudinal diameter FAI of the proximal RCA (10–50 mm), and (e) shows the short-axis FAI, with an overall FAI of  $-95$  HU. (f) displays image noise of  $26$  HU and a pericardial fat attenuation value of  $-97$  HU. (g–i) illustrate CCTA images reconstructed using the filtered back projection (FBP) algorithm. (g) shows the longitudinal diameter FAI of the proximal RCA (10–50 mm), and (h) the short-axis FAI, with an FAI value of  $-97$  HU. (i) demonstrates image noise of  $38$  HU and a pericardial fat attenuation value of  $-97$  HU.

### Coronary CTA image analysis

CCTA image analysis was performed using axial views and curved planar reformation (CPR) to evaluate the proximal  $40$  mm segments of the left anterior descending artery (LAD) and left circumflex artery (LCX), as well as the  $10$ – $50$  mm segment of the right coronary artery (RCA); these are collectively referred to as the proximal

40 mm of the three major coronary arteries. To avoid the potential influence of the aortic wall on the RCA, the analysis for the RCA was limited to the 10–40 mm segment<sup>4</sup>. See Fig. 1.

### Coronary plaque analysis

"The coronary atherosclerotic plaque was defined as a histological structure greater than 1 mm<sup>2</sup>, located within or around the lumen of a coronary artery, and distinct from pericardial tissue, epicardial fat, and the vessel lumen itself. Plaques were quantitatively analysed using post-processing software (CoronaryDoc). Plaque composition was classified as follows: (a) dense calcium, with a density greater than 350 HU; (b) fibrous plaques, with a density ranging from 131 to 350 HU; (c) fibro-fatty plaques, with a density between 31 and 130 HU; and (d) necrotic cores, with a density ranging from –30 to 30 HU<sup>13</sup>.

Based on the percentage of high attenuation components (defined as attenuation components with a plaque density greater than 130 HU<sup>14</sup>) within the proximal 40 mm of the three coronary arteries in the total plaque volume, plaques within this segment were categorised as: non-calcified plaques (high attenuation component percentage < 10%), mixed plaques (10% ≤ high attenuation component percentage < 90%), and calcified plaques (high attenuation component percentage ≥ 90%). A coronary artery was defined as plaque-free if one of the three coronary arteries within 40 mm of the artery showed no plaque, while at least one of the remaining two coronary arteries contained plaque."

### Quantitative analysis of peri-coronary adipose tissue

Peri-coronary FAI was measured automatically using the intelligent analysis software (CoronaryDoc). The long diameter of the region of interest (ROI) was measured as 40 mm proximal to the left anterior descending artery and its echogenic branches, and 10–50 mm proximal to the right coronary artery. The short diameter was determined as the mean diameter of the coronary arteries at the measurement site, with measured densities ranging between –190 and –30 HU in the voxels. FAI was defined as the mean attenuation value of a layer of adipose tissue at a radial distance from the outer wall of the coronary artery equal to the mean diameter of the traced coronary segment<sup>3</sup>. The automated analysis software analysed only voxels within the range of –190 to –30 HU, excluding myocardial tissue adjacent to the vessel wall and coronary branches originating from the target vessel.

### Statistical analysis

The normality of the variables was assessed using the Kolmogorov–Smirnov test. Continuous variables are presented as the mean ± standard deviation, while non-normally distributed variables are expressed as the median with interquartile ranges. Coronary CTA images of the same patient, obtained using different reconstruction algorithms, were analysed using the paired-samples t-test for continuous variables that followed a normal distribution, and the nonparametric Wilcoxon signed-rank test for those that did not. All statistical analyses were conducted using SPSS 20.0 (Chicago, IL, USA), with a *P*-value of < 0.05 considered statistically significant.

## Results

### Baseline data

A total of 773 patients were included in the study, with a mean age of 56 years (range: 24–99 years). Among them, 452 were male (58.58%) and 321 were female (41.52%). The mean height, weight, and BMI of the 773 patients were 166.4 ± 8.2 cm, 70.0 ± 13.4 kg, and 25.1 ± 3.8 kg/m<sup>2</sup>, respectively. Of these patients, 152 (19.66%) had hypertension, 59 (7.63%) had diabetes mellitus, 30 (3.88%) had hyperlipidaemia, and 56 (7.24%) were smokers. A total of 8 patients (1.03%) had a family history of premature coronary artery disease (CAD), which was defined as CAD occurring in the father before the age of 55 or in the mother before the age of 65<sup>15</sup>. See Table 1.

Characteristics	n = 773
Age (years)	56 ± 14
Female sex, n (%)	452(58.58%)
Male sex, n (%)	321(41.52%)
Height(cm)	166.4 ± 8.2
Weight(kg)	70.0 ± 13.4
BMI (kg/m <sup>2</sup> )	25.1 ± 3.8
Coronary artery disease risk factors	
Hypertension (% , n)	152(19.66%)
Diabetes mellitus (% , n)	59(7.63%)
Hyperlipidaemia (% , n)	30(3.88%)
Current smoking (% , n)	56(7.24%)
Family history of CAD (% , n)	8(1.03%)

**Table 1.** Baseline data of patients. Data are presented as mean ± standard deviation or No. (%). BMI, body mass index; CAD, coronary artery disease.

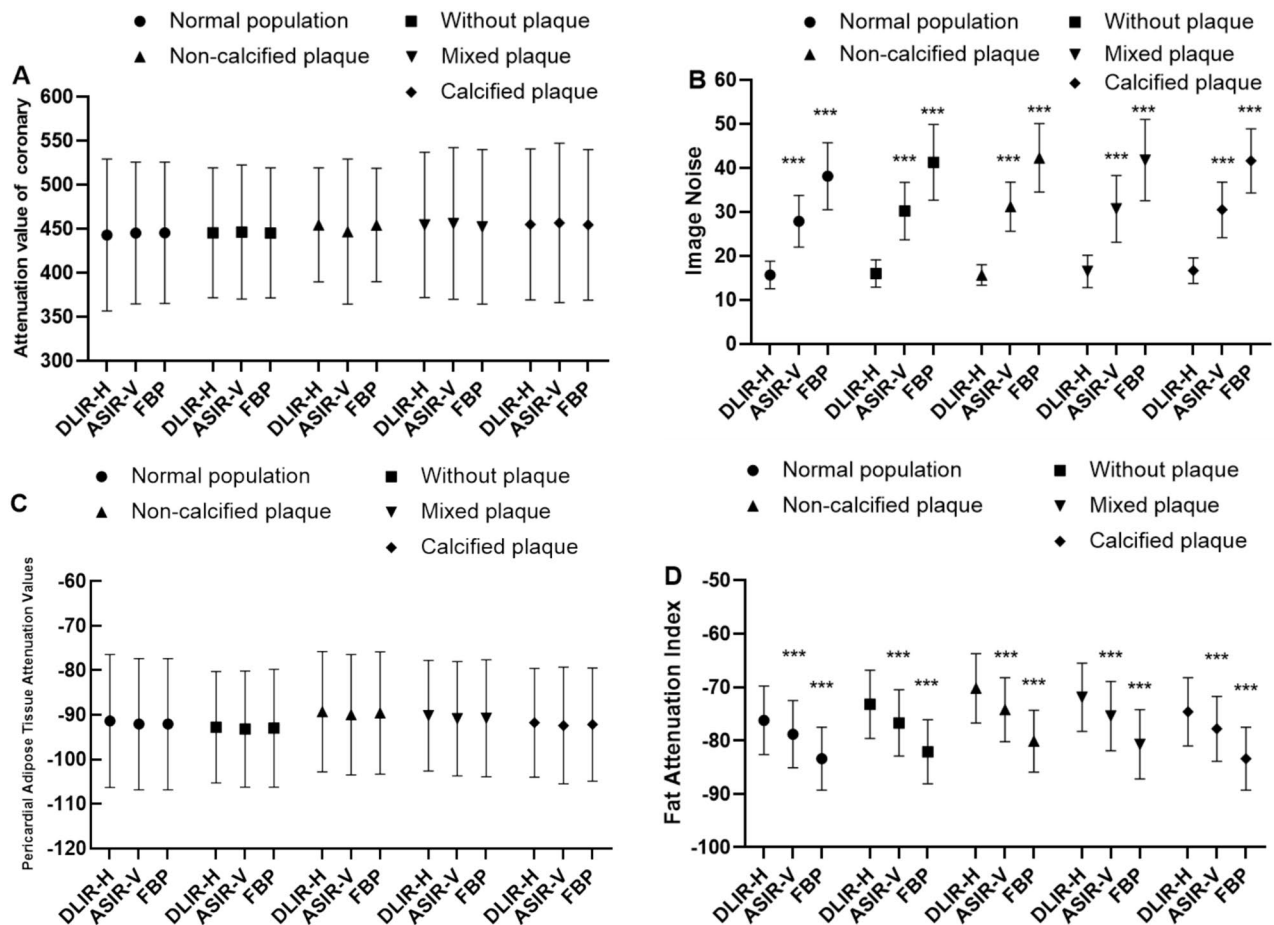


**Fig. 2.** Impact of different reconstruction algorithms on coronary CTA image quality and FAI. (A) demonstrates that reconstruction algorithms have no significant effect on coronary attenuation values (all  $P > 0.05$ ). (B) shows that reconstruction algorithms significantly influence image noise, with DLIR-H achieving the greatest noise reduction, followed by ASiR-V50%, while FBP demonstrates the least noise reduction. These differences were statistically significant (all  $P < 0.001$ ). (C) indicates that there is no significant difference in pericardial fat attenuation values across reconstruction algorithms (all  $P > 0.05$ ). (D) illustrates that reconstruction algorithms significantly affect FAI, with the highest FAI observed in DLIR-H, followed by ASiR-V50%, and the lowest in FBP; all differences were statistically significant (all  $P < 0.001$ ).

In the subgroup analysis, 165 patients were included in the Group normal population, and each of the three subgroups contained 165 patients. The Group without plaque included 212 patients, with 117 in Subgroup RCA, 45 in Subgroup LAD, and 165 in Subgroup LCX. The Group non-calcified plaque included 143 patients, comprising 45 in Subgroup RCA, 59 in Subgroup LAD, and 41 in Subgroup LCX. The Group mixed plaque consisted of 134 patients, with 56 in Subgroup RCA, 98 in Subgroup LAD, and 40 in Subgroup LCX. The Group calcified plaque included 119 patients, with 58 in Subgroup RCA, 53 in Subgroup LAD, and 42 in Subgroup LCX. See Supplementary Tables 1 and 2.

### Comparison of coronary artery attenuation values, image noise, and pericardial fat attenuation across different reconstruction algorithms

#### Coronary artery attenuation values

The coronary artery attenuation values measured using the three reconstruction algorithms—DLIR-H, ASiR-V50%, and FBP—were as follows: In the Group normal population:  $442.9 \pm 86.3$ ,  $445.1 \pm 80.4$ , and  $445.3 \pm 80.2$  HU, respectively. In the Group without plaque:  $445.4 \pm 73.7$ ,  $446.2 \pm 76.1$ , and  $445.2 \pm 73.8$  HU. In the Group non-calcified plaque:  $454.3 \pm 64.7$ ,  $446.7 \pm 82.4$ , and  $454.2 \pm 64.3$  HU. In the Group mixed plaque:  $454.4 \pm 82.5$ ,  $455.9 \pm 86.1$ , and  $452.1 \pm 87.8$  HU. In the Group calcified plaque:  $454.9 \pm 85.7$ ,  $456.7 \pm 90.5$ , and  $454.3 \pm 85.5$  HU. When further subdivided into Subgroup RCA, Subgroup LAD, and Subgroup LCX, no statistically significant differences were observed among the three reconstruction algorithms (all  $P > 0.05$ ). See Fig. 2A and Schedule 1.

### Image noise

The image noise values measured for DLIR-H, ASiR-V50%, and FBP were as follows: In the Group normal population:  $15.7 \pm 3.1$ ,  $27.9 \pm 5.9$ , and  $38.1 \pm 7.6$  HU. In the Group without plaque:  $16.0 \pm 3.1$ ,  $30.2 \pm 6.5$ , and  $41.3 \pm 8.6$  HU. In the Group non-calcified plaque:  $15.7 \pm 2.3$ ,  $31.2 \pm 5.6$ , and  $42.3 \pm 7.8$  HU. In the Group mixed plaque:  $16.5 \pm 3.7$ ,  $30.7 \pm 7.6$ , and  $41.8 \pm 9.2$  HU. In the Group calcified plaque:  $16.7 \pm 2.9$ ,  $30.5 \pm 6.3$ , and  $41.6 \pm 7.3$  HU. When further subdivided into Subgroup RCA, Subgroup LAD, and Subgroup LCX, the differences in image noise among the three reconstruction algorithms were statistically significant in all comparisons (all  $P < 0.001$ ). See Fig. 2B and Schedule 1.

### Pericardial fat CT attenuation values

The pericardial fat CT attenuation values for DLIR-H, ASiR-V50%, and FBP were as follows: In the Group normal population:  $-91.4 \pm 14.9$ ,  $-92.1 \pm 14.7$ , and  $-92.1 \pm 14.7$  HU. In the Group without plaque:  $-92.8 \pm 12.5$ ,  $-93.2 \pm 13.0$ , and  $-93.0 \pm 13.2$  HU. In the Group non-calcified plaque:  $-89.3 \pm 13.5$ ,  $-90.0 \pm 13.5$ , and  $-89.6 \pm 13.7$  HU. In the Group mixed plaque:  $-90.2 \pm 12.4$ ,  $-90.9 \pm 12.8$ , and  $-90.8 \pm 13.1$  HU. In the Group calcified plaque:  $-91.8 \pm 12.2$ ,  $-92.4 \pm 13.1$ , and  $-92.2 \pm 12.7$  HU. Further comparisons across Subgroup RCA, Subgroup LAD, and Subgroup LCX revealed no statistically significant differences among the three reconstruction algorithms (all  $P > 0.05$ ). See Fig. 2C and Schedule 1.

### Comparison of different reconstruction algorithms for coronary FAI

The three reconstruction algorithms, DLIR-H, ASiR-V50%, and FBP, yielded the following FAI values:  $-76.2 \pm 6.4$  HU,  $-78.8 \pm 6.3$  HU, and  $-83.4 \pm 5.9$  HU in the normal population;  $-73.2 \pm 6.4$  HU,  $-76.7 \pm 6.2$  HU, and  $-82.1 \pm 6.0$  HU in the no-plaque group;  $-70.2 \pm 6.5$  HU,  $-74.2 \pm 6.0$  HU, and  $-80.1 \pm 5.8$  HU in the non-calcified plaque group; and  $-71.9 \pm 6.4$  HU,  $-75.4 \pm 6.0$  HU, and  $-80.1 \pm 5.8$  HU in the mixed plaque group. In the calcified plaque group, the FAI values were  $-74.6 \pm 6.4$  HU,  $-77.8 \pm 6.1$  HU, and  $-83.4 \pm 5.9$  HU. Among the three algorithms, FAI measured by the DLIR-H algorithm was the highest, followed by ASiR-V50%, with FBP showing the lowest values. All comparisons were statistically significant (all  $P < 0.001$ ). See Fig. 2D.

Statistically significant differences were also observed in the FAI values measured by the three reconstruction algorithms (DLIR-H, ASiR-V50% and FBP) across subgroups, which included the normal population, no-plaque group, non-calcified plaque group, mixed plaque group, and calcified plaque group, when further subdivided by the right coronary artery, left anterior descending artery, and left circumflex artery branches (all  $P < 0.001$ ). See Schedule 2.

### Discussion

Coronary artery FAI (Fat Attenuation Index) was significantly influenced by the reconstruction algorithm, with DLIR-H yielding the highest FAI values, followed by ASiR-V50%, and the lowest observed under FBP.

With the advancement of computer technology, IR algorithms began to replace FBP as the preferred reconstruction method for CCTA in 2009<sup>16</sup>. However, owing to the non-linear and non-stationary characteristics of IR algorithms, increasing the iterative weighting may gradually lead to a “blotchy” appearance, “waxy” artefacts, and an “unnatural” texture, which can result in the loss of true anatomical details and a decline in image quality. These limitations have restricted the wider application of high-level iterative reconstruction in CCTA<sup>17</sup>. Therefore, when reconstructing images using an IR algorithm at a moderate intensity level of 40% to 60%, a favorable balance between image noise and texture can be achieved, thereby ensuring high-quality images<sup>18</sup>.

Deep Learning Image Reconstruction (DLIR) is a novel AI-based reconstruction algorithm built on deep convolutional neural networks. Trained against high-dose FBP images as the reference standard, it is capable of denoising low-quality, noisy images while preserving true anatomical detail. In doing so, it addresses the “waxy” artefacts and “unnatural” textures commonly associated with high-weight iterative reconstruction. This provides a robust foundation for maintaining high image quality in CCTA performed under low tube voltage conditions, a benefit that has been confirmed by multiple studies<sup>11,19,20</sup>. DLIR offers three reconstruction strength levels: low (DLIR-L), medium (DLIR-M), and high (DLIR-H). De Santis et al.<sup>18</sup>, demonstrated that DLIR-H achieved the lowest image noise (median 9.7, interquartile range 4.5–15.5), comparable to 100% ASiR-V (median 10.4, interquartile range 5.0–17.9,  $P = 1$ ), and significantly lower than DLIR-M, DLIR-L, and all other ASiR-V levels (all  $P \leq 0.021$ ). Accordingly, in this study we selected 50% weighted ASiR-V (ASiR-V50%), high-strength DLIR (DLIR-H), and FBP for image reconstruction under identical tube voltage conditions, aiming to obtain high-quality images while simultaneously evaluating the influence of these three reconstruction algorithms on FAI.

The results of this study indicate that, under the same tube voltage settings, reconstruction algorithms significantly affect FAI measurements in both healthy individuals and patients with coronary plaques. Among the three algorithms, DLIR-H produced the highest FAI values, ASiR-V50% the second highest, and FBP the lowest; all differences were statistically significant. Pericoronary adipose tissue represents a distinct type of fat compared to pericardial fat. While the reconstruction algorithm had a significant impact on the attenuation values of pericoronary fat, it did not affect either the attenuation values of pericardial fat or those of the coronary arteries themselves. Furthermore, the study found that reconstruction algorithms significantly influenced image noise: DLIR-H demonstrated the most substantial noise reduction, whereas FBP was the least effective. There was an inverse relationship between image noise and FAI—lower image noise was associated with higher FAI values. The significant differences in FAI observed among reconstruction algorithms may be attributed to varying degrees of image noise reduction achieved by each method. As noise decreases, image clarity improves, vessel borders become sharper<sup>21</sup>, and the adipose tissue closest to the vascular lumen is better delineated. Since FAI values are higher in regions closer to the vessel lumen than in more distal fat regions<sup>22</sup>, the mean CT attenuation

of perivascular adipose tissue increases accordingly. Among the three algorithms, DLIR-H provided the greatest reduction in image noise, thus resulting in the highest measured FAI values.

However, FAI is influenced by more than just the reconstruction algorithm, and numerous previous studies have shown that FAI values are driven by a variety of factors, including technical, biological, and anatomical elements. Technical factors primarily include the type of CT scanner, tube voltage, and the contrast agent used. Van Diemen et al.<sup>6</sup>, demonstrated a significant difference in FAI between different types of CT scanners, with FAI values of  $-72.2$  HU and  $-80.2$  HU for 64-slice and 256-slice CT scanners, respectively, with  $P < 0.05$ . Tube voltage significantly affects FAI, which is linearly and positively correlated with tube voltage, increasing as the voltage rises<sup>5,23</sup>. FAI is also associated with the presence or absence of contrast injection. Almeida et al.<sup>7</sup>, showed that FAI values were reduced by approximately 3–4 HU in pre-contrast scans compared to post-contrast scans.

Biological factors primarily include gender and body mass index (BMI). van Rosendael et al.<sup>8</sup> demonstrated that FAI was significantly higher in males than in females (LAD:  $-65.7 \pm 7.6$  HU vs.  $-69.4 \pm 7.6$  HU,  $P = 0.014$ ; LCX:  $-60.6 \pm 7.4$  HU vs.  $-64.3 \pm 5.9$  HU,  $P = 0.008$ ; RCA:  $-61.7 \pm 7.9$  HU vs.  $-65.0 \pm 7.7$  HU,  $P = 0.029$ ). Regarding BMI, Antoniadou et al.<sup>9</sup>, concluded that FAI measurements may underestimate coronary inflammation in obese individuals. Overall, adipocyte size is larger in obese individuals (with FAI values closer to  $-190$  HU), whereas in lean individuals, FAI may overestimate coronary inflammation due to the smaller adipocytes, which drive CT attenuation to higher values.

Anatomical factors mainly include variations between different coronary arteries and their respective parts. In the normal population, FAI shows some variability across different coronary arteries. Sugiyama et al.<sup>24</sup>, reported that FAI was  $-72.22 \pm 8.47$  HU in the RCA,  $-71.45 \pm 8.03$  HU in the LAD, and  $-66.80 \pm 7.44$  HU in the left coronary artery. In contrast, based on the DLIR-H algorithm, the FAI in the normal population in this study was  $-78.8 \pm 6.1$  HU in the RCA,  $-77.5 \pm 5.7$  HU in the LAD, and  $-72.4 \pm 5.6$  HU in the LCX. The main difference between the two studies may be attributable to the type of scanner used, as Sugiyama et al. employed a 320-slice CT scanner (Aquilion ONE; Canon Medical Systems Corporation, Otawara, Tochigi, Japan), whereas the present study utilised a 256-slice CT scanner (Revolution APEX CT, GE Healthcare, Waukesha, WI, USA). Finally, with regard to coronary segments, several studies have shown that perivascular FAI is significantly lower in distal coronary artery segments than in proximal ones<sup>10,17,25</sup>.

Several of the studies mentioned above suggest that FAI is influenced by a variety of factors. When FAI is utilised clinically as a biomarker of coronary inflammation, it is crucial to appropriately account for and adjust for technical, biological, and anatomical factors in detecting the presence or absence of inflammation in the coronary arteries, coronary plaque vulnerability, and, in particular, reconstruction algorithms, which have a significant impact on FAI, to ensure accurate assessment of coronary FAI. Moreover, when evaluating the efficacy of pharmacological treatments for coronary artery disease, it is recommended that the same CT scanner and scanning parameters be used to reliably assess changes in FAI before and after treatment.

### Limitations

This study has several limitations. 1. It is a single-centre study with a relatively small sample size. Further multicentre studies with larger datasets are required to validate the impact of different reconstruction algorithms on FAI. 2. Grouping was based on the presence or absence of coronary plaques; however, the influence of reconstruction algorithms on FAI across different sexes and plaque types requires further investigation. 3. This study focused solely on the proximal 40 mm segment of the coronary arteries. Whether other coronary segments are similarly affected by reconstruction algorithms remains to be explored. 4. A standard tube voltage of 120 kV was used in this study. The effect of different reconstruction algorithms on FAI under other tube voltages, particularly lower voltages, needs further in-depth analysis. 5. Patients were grouped only by plaque status. The potential influence of body habitus and variation in coronary attenuation values under the same plaque conditions across different individuals also warrants further investigation.

### Conclusion

In summary, our findings demonstrate that coronary artery FAI is significantly affected by the choice of reconstruction algorithm, with the highest FAI values observed using DLIR-H, followed by ASiR-V50%, and the lowest with FBP. Therefore, in clinical practice, the impact of reconstruction algorithms on FAI should be carefully considered to ensure accurate, reproducible, and comparable FAI measurements.

### Data availability

Data is provided within the supplementary information files.

Received: 13 June 2025; Accepted: 13 November 2025

Published online: 29 December 2025

### References

- Ridker, P. M. et al. Modulation of the interleukin-6 signalling pathway and incidence rates of atherosclerotic events and all-cause mortality: Analyses from the Canakinumab anti-inflammatory thrombosis outcomes study (CANTOS). *Eur. Heart J.* **39**(38), 3499–3507 (2018).
- Goeller, M., Achenbach, S., Duncker, H., Dey, D. & Marwan, M. Imaging of the pericoronary adipose tissue (PCAT) using cardiac computed tomography: Modern clinical implications. *J. Thorac. Imaging* **36**(3), 149–161 (2021).
- Sayeed, R. et al. Detecting human coronary inflammation by imaging perivascular fat. *Sci. Transl. Med.* **9**(398), eal658 (2017).
- Thomas, S. et al. Non-invasive detection of coronary inflammation using computed tomography and prediction of residual cardiovascular risk (the CRISP CT study): A post-hoc analysis of prospective outcome data. *Lancet* **392**(10151), 929–939 (2018).
- Ma, R. et al. Towards reference values of peri coronary adipose tissue attenuation: Impact of coronary artery and tube voltage in coronary computed tomography angiography. *Eur. Radiol.* **30**(12), 6838–6846 (2020).

6. Driessen, R. S. et al. Prognostic value of RCA pericoronary adipose tissue CT-attenuation beyond high-risk plaques, plaque volume, and ischemia. *JACC Cardiovasc. Imaging* **14**(8), 1598–1610 (2021).
7. Birudaraju, D. et al. Feasibility of measuring pericoronary fat from precontrast scans: Effect of iodinated contrast on pericoronary fat attenuation. *J. Cardiovasc. Comput. Tomogr* **14**(6), 490–494 (2020).
8. van Rosendaal, S. E. et al. Vessel and sex differences in pericoronary adipose tissue attenuation obtained with coronary CT in individuals without coronary atherosclerosis. *Int. J. Cardiovasc. Imaging* **38**(12), 2781–2789 (2022).
9. Antoniadis, C., Antonopoulos, A. S. & Deanfield, J. Imaging residual inflammatory cardiovascular risk. *Eur. Heart J.* **41**(6), 748–758 (2020).
10. Antoniadis, C. & Shirodaria, C. Detecting coronary inflammation with perivascular fat attenuation imaging: Making sense from perivascular attenuation maps. *JACC Cardiovasc. Imaging* **12**(10), 2011–2014 (2019).
11. Li, W. et al. High-strength deep learning image reconstruction in coronary CT angiography at 70-kVp tube voltage significantly improves image quality and reduces both radiation and contrast doses. *Eur. Radiol.* **32**(5), 2912–2920 (2022).
12. Etter, D. et al. Towards universal comparability of peri coronary adipose tissue attenuation: A coronary computed tomography angiography phantom study. *Eur. Radiol.* **33**(4), 2324–2330 (2023).
13. Litt, H. et al. Society of cardiovascular computed tomography / North American society of cardiovascular imaging—Expert consensus document on coronary CT imaging of atherosclerotic plaque. *J. Cardiovasc. Comput. Tomogr.* **15**(2), 93–109 (2021).
14. Achenbach, S. et al. Detection of calcified and noncalcified coronary atherosclerotic plaque by contrast-enhanced, submillimeter multidetector spiral computed tomography: A segment-based comparison with intravascular ultrasound. *Circulation* **109**(1), 14–17 (2004).
15. Kaufmann, P. A. et al. Prognostic significance of plaque location in non-obstructive coronary artery disease: From the CONFIRM registry. *Eur. Heart J. Cardiovasc. Imaging* **23**(9), 1240–1247 (2022).
16. Willemink, M. J. & Noel, P. B. The evolution of image reconstruction for CT—from filtered back projection to artificial intelligence. *Eur. Radiol.* **29**(5), 2185–2195 (2019).
17. Greffier, J., Frandon, J., Larbi, A., Beregi, J. P. & Pereira, F. CT iterative reconstruction algorithms: A task-based image quality assessment. *Eur. Radiol.* **30**(1), 487–500 (2020).
18. De Santis, D. et al. Deep learning image reconstruction algorithm: Impact on image quality in coronary computed tomography angiography. *Radiol. Med.* **128**(4), 434–444 (2023).
19. Liu, P. et al. Impact of deep learning-based optimization algorithm on image quality of low-dose coronary CT angiography with noise reduction: A prospective study. *Acad. Radiol.* **27**(9), 1241–1248 (2020).
20. Wang, M. et al. A deep-learning reconstruction algorithm that improves the image quality of low-tube-voltage coronary CT angiography. *Eur. J. Radiol.* **146**, 110070 (2022).
21. Mei, J., Chen, C., Liu, R. & Ma, H. Effect of deep learning image reconstruction on image quality and pericoronary fat attenuation index. *J. Imaging Inform. Med.* **38**, 1881–1890 (2024).
22. Hell, M. M. et al. CT-based analysis of pericoronary adipose tissue density: Relation to cardiovascular risk factors and epicardial adipose tissue volume. *J. Cardiovasc. Comput. Tomogr.* **10**(1), 52–60 (2016).
23. Mergen, V. et al. Epicardial adipose tissue attenuation and fat attenuation index: Phantom study and in vivo measurements with photon-counting detector CT. *AJR Am. J. Roentgenol.* **218**(5), 822–829 (2022).
24. Ohya, H. et al. Determinants of pericoronary adipose tissue attenuation on computed tomography angiography in coronary artery disease. *J. Am. Heart Assoc.* **9**(15), e016202 (2020).
25. Bao, W. et al. A preliminary coronary computed tomography angiography-based study of perivascular fat attenuation index: Relation with epicardial adipose tissue and its distribution over the entire coronary vasculature. *Eur. Radiol.* **32**(9), 6028–6036 (2022).

## Acknowledgements

We would like to express our gratitude to Dr Shuai Zhang, Dr Lei Wang and Dr Aaibin Sun from the GE medical team for the support of this research.

## Author contributions

The authors received no financial support for this work. We declare that this manuscript is original, has not been published before and is not currently being considered for publication elsewhere. We confirm that the manuscript has been read and approved by all named authors and that there are no other persons who satisfied the criteria for authorship but are not listed. We further confirm that the order of authors listed in the manuscript has been approved by all of us. We understand that the Corresponding Author is the sole contact for the Editorial process. She is responsible for communicating with the other authors about progress, submissions of revisions and final approval of proofs. All authors as follows: Zhuyuxuan (First Author): Conceptualization, Data Curation, Formal Analysis, Investigation, Methodology, Software, Visualization, Writing—Original Draft, Writing—Review & Editing; Jiajie Zhu: Methodology, Supervision; Xin Ding: Supervision, Validation; Yingying Ge: Data Curation, Investigation. Dejong Liu: Data Curation, Investigation. Hongbing Ma (Corresponding Author): Conceptualization, Funding Acquisition, Resources, Supervision, Validation, Writing—Original Draft, Writing—Review & Editing.

## Funding

The authors state that this work has not received any funding.

## Declarations

## Competing interests

The authors declare no competing interests.

## Ethics approval

The authors are responsible for all aspects of the work and for ensuring that any issues regarding the accuracy or completeness of the work are properly investigated and resolved. All methods were performed in accordance with the Declaration of Helsinki. The study protocol was approved by the Ethics Committee of BenQ Hospital, Nanjing Medical University, and all participants provided written informed consent prior to participation.

### Additional information

**Supplementary Information** The online version contains supplementary material available at <https://doi.org/10.1038/s41598-025-28914-6>.

**Correspondence** and requests for materials should be addressed to H.M.

**Reprints and permissions information** is available at [www.nature.com/reprints](http://www.nature.com/reprints).

**Publisher's note** Springer Nature remains neutral with regard to jurisdictional claims in published maps and institutional affiliations.

**Open Access** This article is licensed under a Creative Commons Attribution-NonCommercial-NoDerivatives 4.0 International License, which permits any non-commercial use, sharing, distribution and reproduction in any medium or format, as long as you give appropriate credit to the original author(s) and the source, provide a link to the Creative Commons licence, and indicate if you modified the licensed material. You do not have permission under this licence to share adapted material derived from this article or parts of it. The images or other third party material in this article are included in the article's Creative Commons licence, unless indicated otherwise in a credit line to the material. If material is not included in the article's Creative Commons licence and your intended use is not permitted by statutory regulation or exceeds the permitted use, you will need to obtain permission directly from the copyright holder. To view a copy of this licence, visit <http://creativecommons.org/licenses/by-nc-nd/4.0/>.

© The Author(s) 2025